New crystal structure of Nd2Ni7 formed on the basis of stacking of block layers

AUTHOR(S):

Iwatake, Yuki; Okamoto, Norihiko L.; Kishida, Kyosuke; Inui, Haruyuki; Ishida, Jun; Kai, Takuya; Yasuoka, Shigekazu

CITATION:

Iwatake, Yuki ...[et al]. New crystal structure of Nd2Ni7 formed on the basis of stacking of block layers. International Journal of Hydrogen Energy 2015, 40(7): 3023-3034

ISSUE DATE:

2015-02

URL:

http://hdl.handle.net/2433/196058

New Crystal Structure of Nd_2Ni_7 Formed on the Basis of Stacking of Block Layers

Yuki Iwatake[†], *Norihiko L. Okamoto*[†,*], *Kyosuke Kishida*[†], *Haruyuki Inui*[†], *Jun Ishida*[‡], *Takuya Kai*[‡], *and Shigekazu Yasuoka*[‡]

[†]Department of Materials Science and Engineering, Kyoto University
Sakyo-ku, Kyoto 606-8501, Japan

[‡]Technology R & D Division, FDK Twicell Co., Ltd.
307-2 Koyagi-machi, Takasaki, Gunma 370-0071, Japan

***Corresponding Author Contact Information:**

Norihiko L. Okamoto
Department of Materials Science and Engineering, Kyoto University
Sakyo-ku, Kyoto 606-8501, Japan
Tel: +81-75-753-5481
Fax: +81-75-753-5461
E-mail: okamoto.norihiko.7z@kyoto-u.ac.jp

ABSTRACT. The new crystal structure of the intermetallic compound $(Nd,Mg)_2(Ni,Al)_7$ has been determined by scanning transmission electron microscopy and electron diffraction. This crystal structure is different from that (either 2*H* or 3*R*) usually reported for the intermetallic compound R_2T_7 (*R*: rare-earth elements and *T*: transition-metal elements) in the constitution of block layers. While the block layer for the crystal structure usually reported is of the R_2T_7 stoichiometric composition consisting of one R_2T_4 unit layer and two RT_5 unit layers, the block layer for the new crystal structure consists of a sub-block layer of the RT_3 stoichiometry (formed with one R_2T_4 unit layer and one RT_5 unit layer) and a sub-block layer of the R_5T_{19} stoichiometry (formed with one R_2T_4 unit layer and three RT_5 unit layers), which alternately stack on top of each other. The crystal structure is described based on the order-disorder (OD) theory and the simplest crystal structures (polytypes) among many other polytypes belonging to the same OD family is deduced to be of the 2*H*-type with the space group of $P\bar{6}m2$ and of the 6*R*-type with the space group of $R\bar{3}m$. The experimentally observed polytype corresponds to the second simplest form of the 6*R*-type.

KEYWORDS. Hydrogen storage material, Order-disorder (OD) theory, Polytype, Scanning transmission electron microscopy, Superlattice structure, La_2Ni_7

1. INTRODUCTION

Since the discovery of the excellent hydrogen absorption-desorption properties in 2000 [1], the intermetallic compound based on R_2T_7 (R: rare-earth elements and T: transition-metal elements) has received a considerable interest not only scientifically [2-9] but also industrially [10]. This stems from the fact that the additions of Mg completely alter the hydrogen absorption-desorption properties of La_2Ni_7 [1], which had been believed to exhibit properties not useful for the application as negative electrode materials of rechargeable nickel-metal hydride (Ni-MH) batteries because of the occurrence of non-rechargeable amorphization upon hydrogenation at ambient temperature [11]. Since then, many studies have devoted to the intermetallic compound based on R_2T_7, such as La_2Ni_7 and $(La,Mg)_2Ni_7$ in order to develop alloys that exhibit better hydrogen absorption-desorption properties as negative electrode materials of rechargeable Ni-MH batteries. One of the focuses in the alloy development has been to establish the structure-properties relationships, paying special attention to the control of phase constitution, crystal structure (polytype) by alloying additions and their preferential sites. One of the most significant scientific characteristics in the intermetallic compound based on R_2T_7 is in its crystal structure, as in other series compounds. The unit cells of a series of compounds in the R-T system, RT_3, R_2T_7 and R_5T_{19} are known to be made of some block layers, each consisting of one unit layer of the R_2T_4 (Laves)-type and some unit layers of the RT_5-type [12-14] (Fig. 1). The number (n) of RT_5-type unit layers in a block layer is 1, 2 and 3 for RT_3, R_2T_7 and R_5T_{19}, respectively. Thus, this series of compounds are formulated to be RT_x with $x=(5n+4)/(n+2)$ [12]. Of significance to note is that for all these compounds RT_x, each block layer possesses the stoichiometric composition of the corresponding intermetallic compound and that depending on the stacking of these block layers, some different polytypes (such as 2H and 3R according to the Ramsdell notation [15]) are generated for each of these

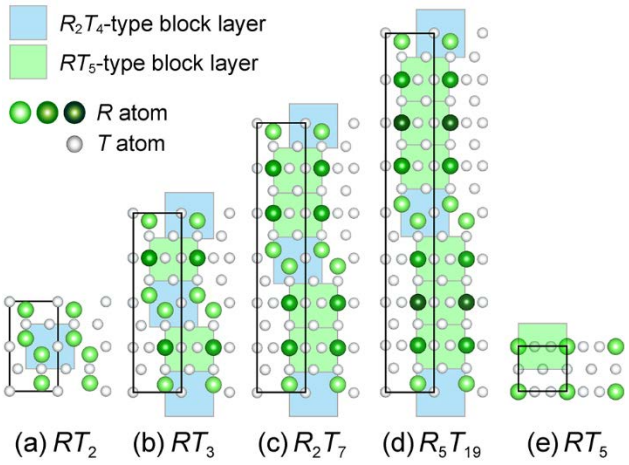

Figure 1. Crystal structures of (a) RT_2 (R_2T_4), (b) RT_3, (c) R_2T_7, (d) R_5T_{19} and (e) RT_5. RT_2 and RT_5 have C15 (Laves)- and $CaCu_5$-type structures, respectively. The crystal structures of (b) RT_3, (c) R_2T_7 and (d) R_5T_{19} consist of block layers, each of which consists of R_2T_4 and RT_5 unit layers, and the polytype *2H* is illustrated for these intermetallics.

compounds RT_x (Fig. 1). During the course of research on the development of alloys based on the intermetallic compound R_2T_7, we have recently found a new crystal structure for the R_2T_7 phase in the Nd-Mg-Ni-Al quaternary system, the crystal structure of which cannot simply be described according to the above-mentioned method with the stacking of block layers possessing the stoichiometric composition of the corresponding intermetallic compound.

In the present paper, we report the results of crystal structure assessment made for the R_2T_7 phase in the Nd-Mg-Ni-Al quaternary system by means of high-resolution scanning transmission electron microscopy (STEM) as well as electron diffraction. We describe the crystal structure based on the order-disorder (OD) theory [16-21] and deduce the simplest crystal structures (polytypes) of many other polytypes belonging to the same OD family, together with their space groups.

2. EXPERIMENTAL PROCEDURES

Two different Nd-Mg-Ni-Al quaternary alloys (1 and 2) were prepared by induction-melting the constituent elements in their desired molar fractions, followed by annealing at 950 °C for 48 h in Ar gas and furnace-cooling. The molar ratio of (Nd+Mg):(Ni+Al) was set at 2:7 for both alloys, assuming all Nd and Mg atoms occupy the *R* sites while all Ni and Al atoms occupy the *T* sites in the intermetallic compound R_2T_7. The alloy 2 contains less Nd and more Mg than the alloy 1, as tabulated in Table 1. Microstructures (phase constitution) and their crystal structures in these alloys were examined with JEM-2100F scanning transmission electron microscope (STEM) operated at 200 kV. Phase compositions were examined by energy-dispersive spectroscopy (EDS) in the STEM. Thin foils for STEM observations were perforated by ion milling with 3 keV Ar ions.

Table 1. Nominal compositions of the alloys 1 and 2.

(at.%)	Nd	Mg	Ni	Al
Alloy 1	16.7	5.6	74.4	3.3
Alloy 2	15.6	6.7	74.4	3.3

3. RESULTS

The alloy 1 consists of four phases, R_2T_7, R_5T_{19}, RT_5 and RT_2, with R_2T_7 being the major constituent phase. Figures 2(a) and (b) show a typical high-resolution HAADF (high-angle annular dark-field)-STEM image and a selected-area electron diffraction (SAED) pattern with the $[2\bar{1}\bar{1}0]$ incidence of a crystal grain of the R_2T_7 phase. EDS analysis indicates that the chemical composition of the R_2T_7 phase is on average Nd-2.1Mg-79.5Ni-1.4Al (at.%). The R_2T_7 phase of Fig. 2(a) consists of

block layers of the R_2T_7 stoichiometric composition formed with one R_2T_4 unit layer and two RT_5 unit layers. These block layers stack in the *c*-axis direction so as to form the AB-type stacking (2*H* polytype), as schematically illustrated in the inset of Fig. 2(a). Stacking faults (the disturbance of the AB-type stacking as well as the intergrowth of other phases with different block layer structures) were observed only sporadically in grains of the R_2T_7 phase. The SAED pattern of Fig. 2(b) is consistently indexed as that of R_2T_7 of the 2*H* polytype. The discreteness of diffraction spots together with the absence of streaks in the SAED pattern of Fig. 2(b) is consistent with the high-resolution STEM image of Fig. 2(a) showing a very regular AB-type stacking (2*H* polytype) of the R_2T_7 phase without stacking faults.

The alloy 2 also consists of four phases, R_2T_7, RT_5, RT_3 and RT_2, with R_2T_7 being the major constituent phase. EDS analysis indicates that the chemical composition of the R_2T_7 phase is on average Nd-5.6Mg-77.2Ni-2.9Al (at.%), which is a little more in Mg and Al than in the R_2T_7 phase in the alloy 1. Figures 3(a) and (b) show a typical high-resolution HAADF-STEM image and a SAED pattern with the $[2\bar{1}\bar{1}0]$ incidence of a crystal grain of the R_2T_7 phase. The SAED pattern of Fig. 3(b) is completely different from that of the R_2T_7 phase of the 2*H* polytype. Analysis of the stacking of block layers in Fig. 3(b) indicates that unlike in the R_2T_7 phase ever reported, the block layer of this R_2T_7 phase consists of a block layer of the RT_3 stoichiometry (formed with one R_2T_4 unit layer and one RT_5 unit layer) and that of the R_5T_{19} stoichiometry (formed with one RT_3 unit layer and three RT_5 unit layers) alternately stacked on top of each other. This new R_2T_7 phase is thus described to consist of the block layer of the R_2T_7 stoichiometry formed with alternatively stacked sub-block layers of the RT_3 and R_5T_{19} stoichiometries. The R_2T_7 block layer stacks in the *c*-axis direction so as to form the ABC-type stacking to complete the

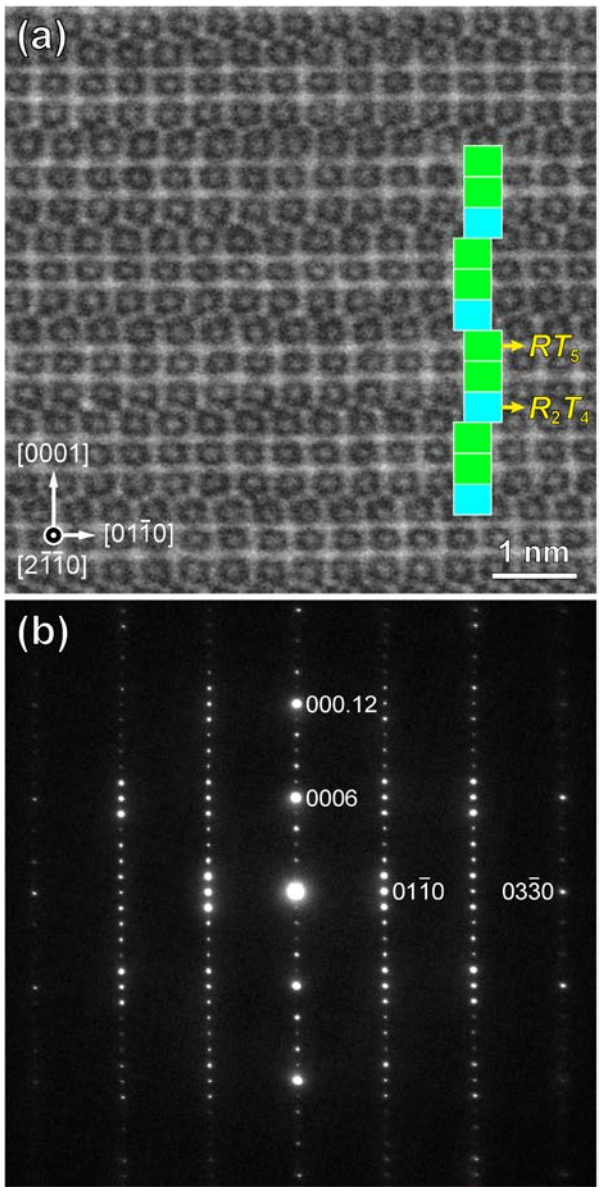

Figure 2. (a) Typical high-resolution HAADF-STEM image and (b) SAED pattern with the [2$\bar{1}\bar{1}$0] incidence for a crystal grain of the R_2T_7 phase in the alloy 1.

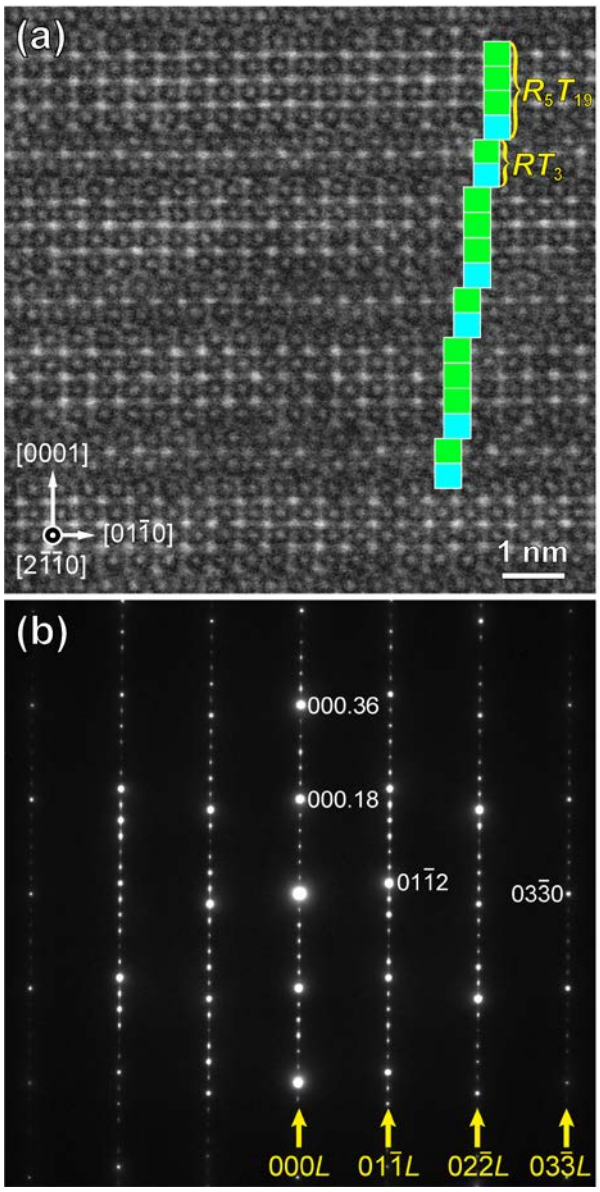

Figure 3. (a) Typical high-resolution HAADF-STEM image and (b) SAED pattern with the [2$\bar{1}\bar{1}$0] incidence for a crystal grain of the R_2T_7 phase in the alloy 2.

three-layer unit cell, as schematically shown in the inset of Fig. 3(a). The ABC-type three-layer stacking is usually observed for this R_2T_7 phase and seems the lowest energy configuration. The space group of $R\bar{3}m$ can thus be assigned to this new crystal structure. The SAED pattern of Fig.

3(b) is consistently indexed with the assigned space group of $R\bar{3}m$ for the new crystal structure of the R_2T_7 phase. Although the crystal structure can also be considered as an intergrowth structure of the RT_3 and R_5T_{19} phases, we believe the structure is regarded as a new crystal structure in view of the very regularity of the incidence of sub-block layers of the RT_3 and R_5T_{19} stoichiometry and rather wide areas of the appearance of the structure, as shown in a low-magnification HAADF-STEM image of Fig. 4. Being consistent with the occurrence of streaks in the SAED pattern of Fig. 3(b), the incidence of stacking faults SF1 and SF2 are observed in Fig. 4, although the density of stacking faults is not generally remarkably high in other areas. A sub-block layer of the R_5T_{19} stoichiometry is missing for the stacking faults SF1, while for the stacking fault SF2, a sub-block layer of the RT_3 stoichiometry is missing. Stacking fault between adjacent block layers of the R_2T_7 stoichiometry to disturb the ABC-type three-layer stacking of the new crystal structure is rarely observed. In the same specimen, crystal grains of the R_2T_7 phase with the well-known crystal

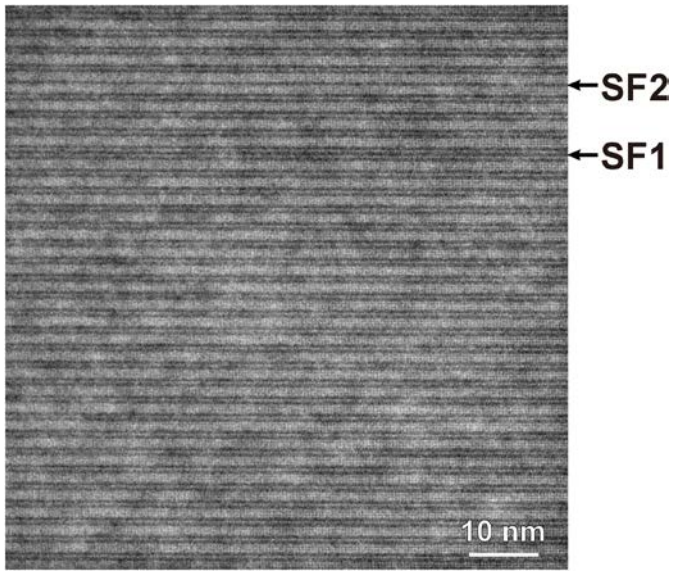

Figure 4. Low-magnification HAADF-STEM image of the R_2T_7 phase in the alloy 2. Positions of stacking faults (SF1 and SF2) are indicated in the right of the figure.

structure of the 2*H* polytype (space group $P6_3/mmc$) are also frequently observed. These grains tend to have chemical compositions with less Mg and Al than grains of the R_2T_7 phase with the new crystal structure, although the difference in chemical composition is not always remarkable.

4. DISCUSSION

4.1. The crystal structure description of RT_3, R_2T_7 and R_5T_{19} with the order-disorder theory

Although two polytypes, 2*H* and 3*R* are frequently described to be observed experimentally for a series of compounds in the *R*-*T* system, RT_3, R_2T_7 and R_5T_{19}, many other polytypes with larger unit cell dimensions along the stacking direction as well as virtually one-dimensionally stacking disordered structures are possible to be formed, since their unit cell is based on the stacking of block layers, each of which consists of one unit layer of the RT_2 (Laves)-type and some unit layers of the RT_5-type. Here, we describe the crystal structures of a series of compounds in the *R*-*T* system (RT_3, R_2T_7 and R_5T_{19}) according to the so-called order-disorder theory [16-21] in order to generalize the crystal structures. The theory of the OD structure (OD theory) was originally developed to describe crystal structures with one-dimensional stacking disorder observed in many minerals, such as wollastonite [22-27]. In the OD theory, a crystal structure is described with two sets of partial operations (POs) of symmetry, λ-POs and σ-POs [16-21]. The λ-POs correspond to POs that transform an OD layer into itself, while σ-PO transforms an OD layer into an adjacent one above it. For a given set of λ-POs, i.e. a given layer group, a set of σ-POs can be derived based on the symmetry of the layer group. The POs sustaining the orientation of the layer are denoted as τ-POs, while those turning the layer upside down are called ρ-POs. Both λ- and σ- POs can be either τ or ρ. A whole family of the derivative

structures described with a complete set of POs is called an OD-groupoid family.

The choice of OD layers in the crystal structure description according to the OD theory is not unique and there are some different possibilities. The block layer with the stoichiometric composition (either RT_3, R_2T_7 or R_5T_{19}) is one of them. The structural block can indeed be divided into two different OD layers corresponding respectively to sub-block layers of the R_2T_4 (Laves)- and the RT_5-types, as shown in Figs. 5(a)-(c). This choice of OD layers is convenient to describe the crystal structures of these three intermetallic compounds in a quite similar way according to the OD theory. These two different OD layers are denoted in the following as L_n and M_n:

(i) OD layer L_n, corresponding to a sub-block layer of the R_2T_4-type (Figs. 5(a)-(c) and 6(a)-(b)). The layer group of the OD layer L_n is $p\bar{3}m1$ (short symbol) or $Pmmm(\bar{3})111$ (full seven-entry symbol). The layer is non-polar. There is one λ-ρ plane.

(ii) OD layer M_n, corresponding to a sub-block layer of the RT_5-type (Figs. 5 (a)-(c) and 6 (c)-(f)). This OD layer contains all unit layers of the RT_5-type in the sub-block layer for each of these three compounds. Thus, the number of unit layers of the RT_5-type contained in the OD layer is 1, 2 and 3 for RT_3, R_2T_7 and R_5T_{19}, respectively. The number of unit layers of the RT_5-type contained in the OD layer does not alter the symmetry of the OD layer. The layer group of the OD layer M_n is $p6/mmm$ (short symbol) or $Pmmm(6/m)mmm$ (full seven-entry symbol). The layer is non-polar. There is one λ-ρ plane.

The crystal structures of these three intermetallic compounds can thus be considered to consist of these two OD layers stacked alternately along the c direction. The diagrams of symmetry elements for the $p\bar{3}m1$ and $p6/mmm$ layer groups corresponding to the λ-POs in the OD layers L_n and M_n are illustrated in Figs. 6(g) and (h), respectively [28]. Because the crystal structure is composed of

two OD layers both of which are non-polar (as is evident from the presence of λ-ρ plane), all the three intermetallics can be considered to belong to the category IV OD structures [20, 29-31]. The

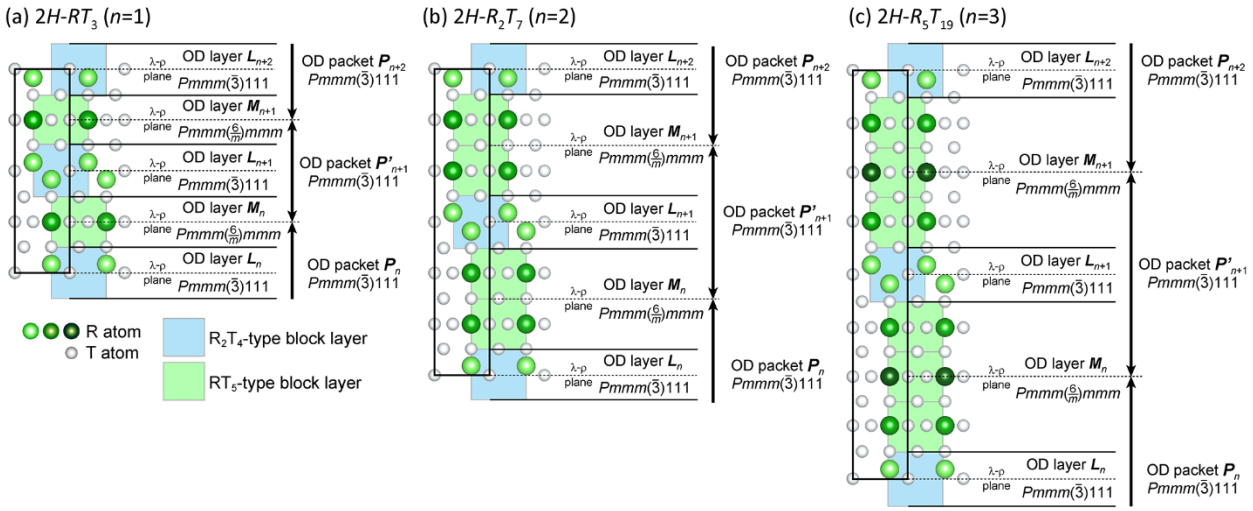

Figure 5. Crystal structures of (a) 2*H*-RT_3, (b) 2*H*-R_2T_7, and (c) 2*H*-R_5T_{19} projected along the [2 1 1 0] direction. The constituting OD layers and packets are described in the right-hand of each figure.

choice of OD layers in OD structures of the category IV is not unique and a boundary between two adjacent OD layers can be set in more than one way [20]. Here, the boundary between two adjacent L_n and M_n OD layers is set so that *T* atoms on the boundary (highlighted with light blue color in Fig. 6) belong to both OD layers.

The so-called *NFZ* relation [18, 20, 21] is useful to consider the number of geometrically equivalent stacking positions of the OD layers. The *NFZ* relation calculates the value of *Z*, the number of the possible distinct positions of the OD layer L_{p+1} relative to the fixed position of the OD layer L_p. The value of *Z* depends on the order *N*, the general multiplicity of the group of the λ-τ-POs valid for the single OD layer L_p, as well as on the order *F*, the general multiplicity of the group of the λ-τ-POs valid both for the single OD layer L_p and for the pair of the adjacent OD

layers L_p and L_{p+1}. For OD structures in the category IV, the value of Z is calculated through the relation, $Z = N/F$. In the case for stacking an OD layer M_n on top of an OD layer L_n , the order N for the OD layer L_n is six out of 12 symmetry operations of the $p\bar{3}m1$ layer group [28]. Since all the six operations are valid for the pair of the adjacent OD layers L_n and M_n, the order F is also six. Thus, the number $Z = N/F = 6/6 = 1$, indicating that there is only one possible position for the OD layer M_n to stack on top of the OD layer L_n. In the case for stacking an OD layer L_{n+1} on top of that an OD layer M_n, on the other hand, the order N for the OD layer M_n is 12 out of 24 symmetry operations of the $p6/mmm$ layer group [28]. Since only six out of the 12 operations are valid for the pair of the adjacent OD layers M_n and L_{n+1}, the order F is also six. Thus, the number $Z = N/F = 12/6 = 2$. This indicates that there are two possible stacking positions when stacking an OD layer L_{n+1} on top of that an OD layer M_n.

The symmetry of an OD structure is not described by a space group but is by a groupoid, which is a set of λ- and σ-POs [16-21]. A whole family of derivative structures described with the

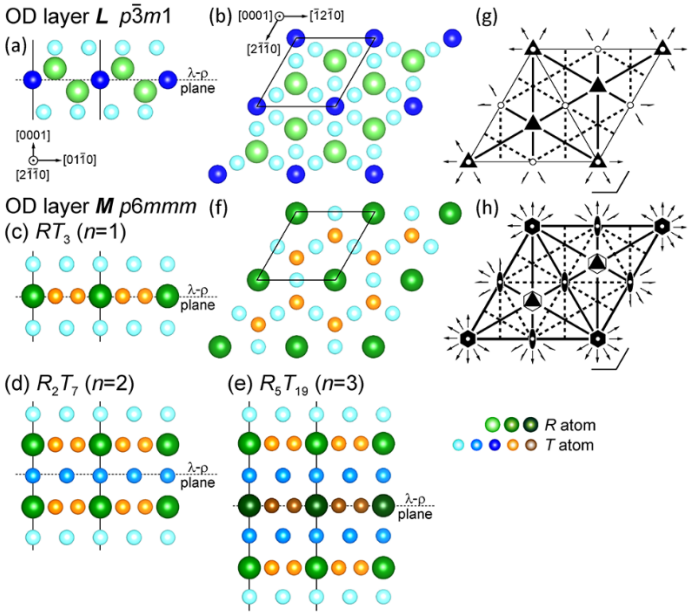

Figure 6. (a,c,d,e) $[2\bar{1}\bar{1}0]$ and (b,f) [0001] projections of the OD layers (a,b) *L* and (c,d,e) *M*, respectively, in the (c) RT_3, (d) R_2T_7, and (e) R_5T_{19} phases. (g,h) Diagrams of symmetry elements for the $p\bar{3}m1$ and $p6/mmm$ layer groups corresponding to the λ-POs in the OD layers *L* and *M*, respectively.

same set of λ- and σ-POs is called an OD groupoid family and is generally described with the so-called OD-groupoid family symbol, which consists of two lines [16-21]. For the OD structures in the category IV composed of two different kinds of OD layers, the first line presents the λ-POs of the layer groups of the constituting OD layers, while the second line presents the positional relation between the adjacent OD layers, given in a square bracket by two components of the vector connecting the origins of the two adjacent layers projected into the layer plane [20, 21, 29-31]. The OD groupoid family symbol for all three intermetallics is thus described as,

$$Pmmm\left(\frac{6}{m}\right)mmm \quad Pmmm(\bar{3})11 \qquad [2/3,1/3] \tag{1}$$

Of significance to note is that the OD groupoid family symbol is the same for all three intermetallics and does not alter with the thickness (the number of unit layers of the RT_5-type) of the OD layer M_n.

It is often more instructive and useful to describe OD structures with structural units called OD packets, which by definition represent the smallest continuous part of the OD structure with the stoichiometric composition and is larger than individual OD layers considered previously [32]. The OD packet consists of half the OD layer $M_{n\text{-}1}$, the whole OD layer L_n and half the OD layer M_n with the packet boundaries being taken to coincide with the λ-ρ plane of the OD layers $M_{n\text{-}1}$ and M_n (Figs. 5 and 7(a)). The OD packet P_n is thus virtually identical with the structural blocks used for explaining the crystal structures in Section 1, although the packet boundary is shifted by half the OD layer M_n when compared with that between structural blocks. Here, the boundary

between two adjacent OD packets is set so that *R* and *T* atoms on the λ-ρ plane in the OD layer M_n belong to both OD packets (highlighted with green and orange color in Fig. 6(c), cyan color in Fig.

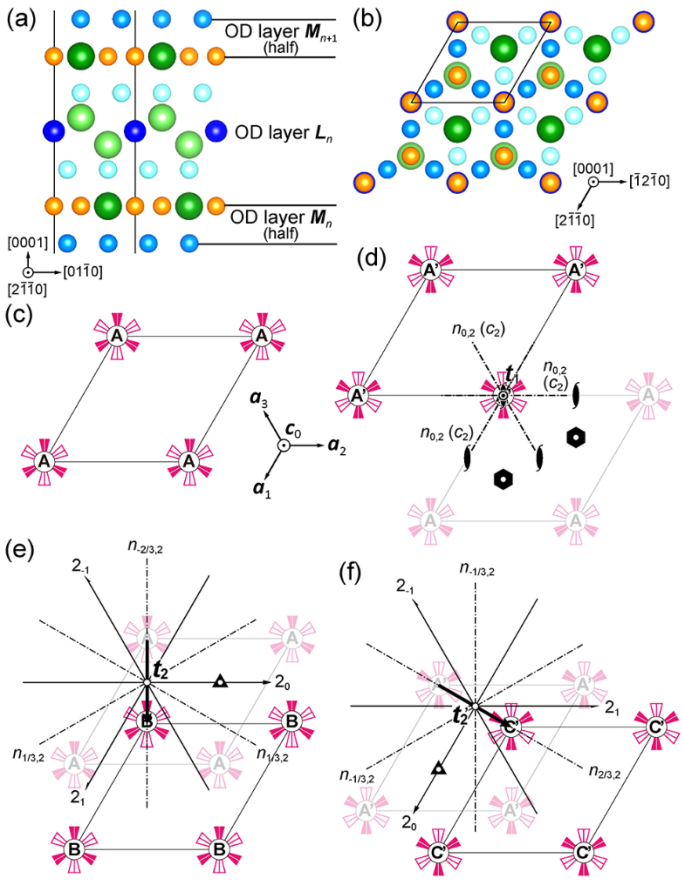

Figure 7. (a) [2$\bar{1}\bar{1}$0] and (b) [0001] projections of the OD packet in the R_2T_7 phase. (c) Arrays of symbolic figures showing the symmetry of the OD packet. (d,e) Two different manners of stacking the adjacent OD packet on the preceding OD packet at the position A. (d) A⇒A' with the stacking vector $\boldsymbol{t}_1$, (e) A⇒B with the stacking vector $\boldsymbol{t}_2$. (f) One of the two manners of stacking the adjacent OD packet on the preceding OD packet at the position A' (A'⇒C').

6(d), and dark green and brown color in Fig. 6(e), respectively). The symmetry of the OD packet for all three intermetallics is identical with the symmetry of the OD layer L_n, $p\bar{3}m1$. It is useful to further describe the OD packet with a symbolic figure, which simply illustrates the symmetry of the OD packet [33]. The OD packet projected along the stacking direction and symbolic figure for

the OD packet are shown in Figs. 7(b) and (c), respectively. The symbolic figure has $\bar{3}$ symmetry about the stacking direction and mirror planes perpendicular to the <11$\bar{2}$0> directions. The origin of the adjacent packet P_{n+1} may be shifted relative to that of the packet P_n by either of the following stacking vectors,

$$\boldsymbol{t}_1 = \boldsymbol{c}_0 \tag{2a}$$

$$\boldsymbol{t}_2 = \frac{2}{3}\boldsymbol{a}_1 + \frac{1}{3}\boldsymbol{a}_2 + \boldsymbol{c}_0 \tag{2b}$$

where $\boldsymbol{c}_0$ corresponds to the unit vector of the OD packet along the stacking direction. In the former case, the packet P_{n+1} is stacked right above the packet P_n after ±60 or 180° rotation about the *c*-axis (A→A': Fig. 7(d))[1]. In the latter case, the packet P_{n+1} is stacked obliquely above the packet P_n without rotation (A→B: Fig. 7(e)). When the packet P_n has a different orientation (±60 or 180° rotation about the *c*-axis; A' position), the packet P_{n+1} can be stacked right above the packet P_n after ±60 or 180° rotation about the *c*-axis (A'→A), after shifting the origin by the following stacking vector,

$$\boldsymbol{t}'_1 = \boldsymbol{c}_0, \tag{2c}$$

or obliquely above the packet P_n without rotation (A'→C': Fig. 7(f)) after shifting the origin by the following stacking vector,

$$\boldsymbol{t}'_2 = \frac{1}{3}\boldsymbol{a}_1 + \frac{2}{3}\boldsymbol{a}_2 + \boldsymbol{c}\,. \tag{2d}$$

[1]The apostrophe means that the OD packet has the opposite orientation within the basal plane.

The stacking vector $\boldsymbol{t}_1$ shifts the stacking positions like A→A', B→B', C→C', while $\boldsymbol{t}_2$ and $\boldsymbol{t}'_2$ shift the stacking positions like A→B, B→C, C→A, and A'→C', B'→A', C'→B', respectively. An infinite number of periodic and non-periodic polytypes can thus be obtained for these three intermetallics (RT_3, R_2T_7 and R_5T_{19}) by a random occurrence of the stacking vectors $\boldsymbol{t}_i$ and $\boldsymbol{t}'_i$ (i = 1 and 2).

Among the periodic polytypes, the simplest ones are called maximum degree of order (MDO) polytypes. Each MDO polytype is characterized by a generating operation, whose continuous application gives rise to the MDO structure. In the present case of the OD groupoid family for RT_x with x=(5n+4)/(n+2), one generating operation is the σ-PO of $n_{0,2}$ (c_2), indicated in Fig. 7(d). Continuous application of this operation yields an MDO polytype (MDO1) with the AA' stacking sequence. The unit cell of the MDO1 polytype belongs to the space group of $P6_3/mmc$ with a hexagonal unit cell of $\boldsymbol{a}_1^{(MDO1)} = \boldsymbol{a}_1$, $\boldsymbol{a}_2^{(MDO1)} = \boldsymbol{a}_2$ and $\boldsymbol{c}^{(\mathrm{MDO1})} = 2\boldsymbol{c}_0$ because the σ-PO of $n_{0,2}$ (c_2) (Fig. 7(d)) becomes a total operation, c glide plane, in the hexagonal cell. In the Ramsdell notation, the MDO1 polytype is designated 2H. Another generating operation is the σ-PO of a glide plane of $n_{1/3,2}$, indicated in Fig. 7(e). Continuous application of this operation results in another MDO polytype (MDO2) with the ABC stacking sequence. The MDO2 polytype belongs to the space group of $R\bar{3}m$ with the rhombohedral unit cell of $\boldsymbol{a}_1^{(MDO2)} = \boldsymbol{a}_1$, $\boldsymbol{a}_2^{(MDO2)} = \boldsymbol{a}_2$ and $\boldsymbol{c}^{(\mathrm{MDO2})} = 3\boldsymbol{c}_0$ because the σ-PO of $n_{1/3,2}$ becomes a total operation, g(1/6, 1/3, 1/3), in the rhombohedral cell. In the Ramsdell notation, the MDO2 polytype is designated 3R.

4.2. The crystal structure description of R_2T_7 of the new crystal structure with the order-disorder theory

We now describe the new crystal structure of R_2T_7 we identified presently with the OD theory. Although it is possible to choose OD layers as in the previous section (Figs. 5, 6, and 7), the crystal structure description is rather complicated because the structural block with the R_2T_7 stoichiometric composition consists of as many as three different kinds of OD layers (L_{4n}, M_{4n+1}, L_{4n+2} and M'''_{4n+3}, with M_{4n+1} and M'''_{4n+3} containing one and three unit layers of the RT_5-type, respectively). To simplify the description, two different kinds of OD layers can be chosen as follows.

(i) OD layer L' (L'_{3n} and L'_{3n+1}), consisting of a R_2T_4-type unit layer sandwiched by half the RT_5-type unit layer on both sides (top and bottom) (Fig. 8 and Figs. 9(a), (b)). The layer group of the OD layer L' is $p\bar{3}m1$ (short symbol) or $Pmmm(\bar{3})111$ (full seven-entry symbol). The layer is non-polar. There is one λ-ρ plane.

(ii) OD layer M' (M'_{3n+2}), consisting of a RT_5-type unit layer sandwiched by half the RT_5-type unit layer on both sides (top and bottom), i.e., two RT_5-type unit layers (Fig. 8 and Figs. 9(c), (d)). The layer group of the OD layer M'_{3n+2} is $p6/mmm$ (short symbol) or $Pmmm(6/m)mmm$ (full seven-entry symbol). The layer is non-polar. There is one λ-ρ plane.

Then, the structural block with the R_2T_7 stoichiometric composition can simply be described to consist of OD layers L'_{3n}, L'_{3n+1} and M'_{3n+2}. In the case for stacking an OD layer L'_{3n} on top of an OD layer M'_{3n-1}, the order N for the OD layer M is 12 out of 24 symmetry operations of the $p6/mmm$ layer group [28]. Since only six out of the twelve operations are valid for the pair of the adjacent OD layers M'_{3n-1} and L'_{3n}, the order F is also six. Thus, the number $Z = N/F = 12/6 = 2$, indicating that the existence of two possible stacking positions for the OD layer L'_{3n} to stack on top of the OD layer M'_{3n-1}. In the case for stacking an OD layer L'_{3n+1} on top of an OD layer L'_{3n}, the order N for the OD layer L'_{3n} is six out of 12 symmetry operations of the $p\bar{3}m1$ layer group

[28]. Since only three out of the six operations are valid for the pair of the adjacent OD layers L'_{3n}, and L'_{3n+1}, the order F is also three. Thus, the number $Z = N/F = 6/3 = 2$, indicating that the existence

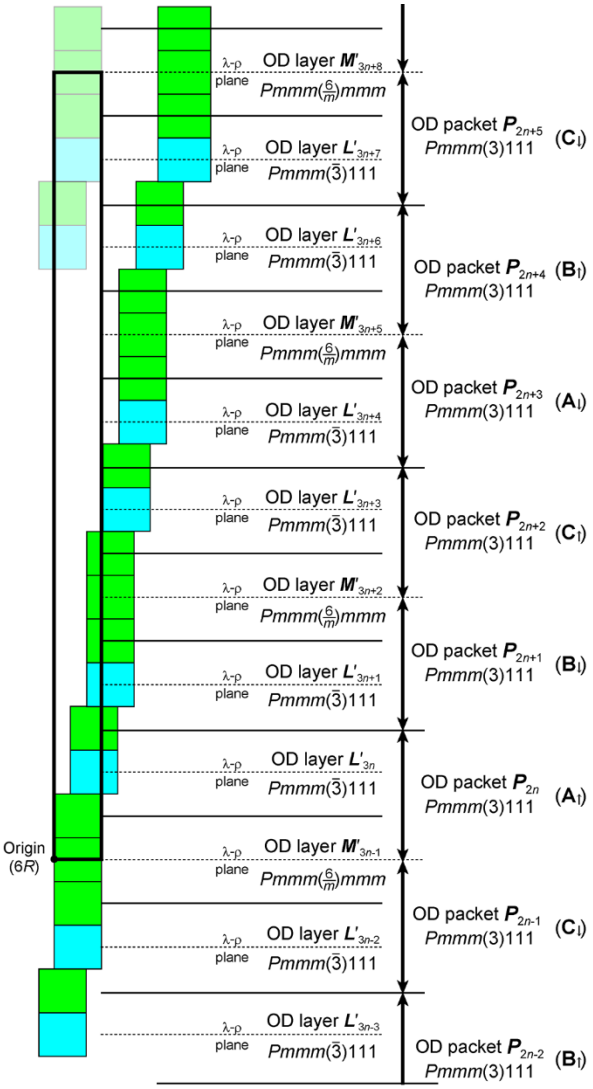

Figure 8. Schematic illustration of the crystal structure of the intermetallic compound $(Nd,Mg)_2(Ni,Al)_7$ (6*R*-polytype). The constituting OD layers and packets are described in the right-hand of the figure.

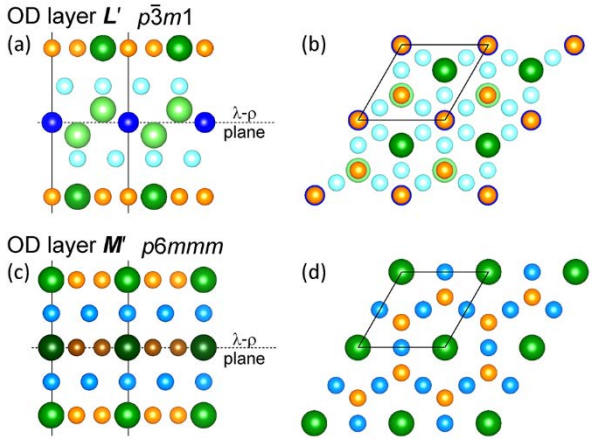

Figure 9. (a,c) $[2\bar{1}\bar{1}0]$ and (b,d) [0001] projections of the OD layers (a,b) L' and (c,d) M', respectively, in the $(Nd,Mg)_2(Ni,Al)_7$ phase of the new crystal structure.

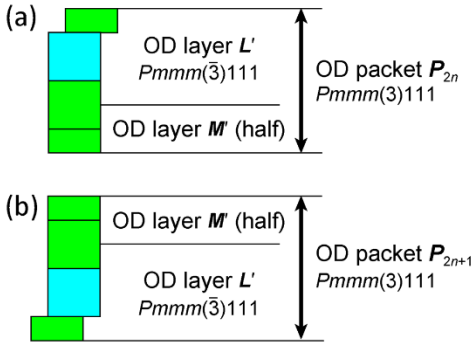

Figure 10. Schematic illustration of the OD packets P_{2n} and P_{2n+1} constituting the $(Nd,Mg)_2(Ni,Al)_7$ phase of the new crystal structure.

of two possible stacking positions for the OD layer L'_{3n+1} to stack on top of the OD layer L'_{3n}. In

the case for stacking an OD layer M'_{3n+2} on top of an OD layer L'_{3n+1}, on the other hand, the order N for the OD layer L'_{3n+1} is six out of 12 symmetry operations of the $p\bar{3}m1$ layer group. Since all the six operations are valid for the pair of the adjacent OD layers L'_{3n+1} and M'_{3n+2}, the order F is also six. Thus, the number $Z = N/F = 6/6 = 1$, indicating that there is only one possible position for the OD layer M'_{3n+2} to stack on top of the OD layer L'_{3n+1}. Because the crystal structure is composed of three OD layers all of which are non-polar (as is evident from the presence of λ-ρ plane), the structure can be considered to belong again to the category IV OD structures [20, 29-31]. The OD groupoid family symbol for the crystal structure is thus described as,

$$\underset{[2/3,1/3]}{Pmmm\left(\frac{6}{m}\right)mmm} \quad \underset{[2/3,1/3]}{Pmmm(\bar{3})11} \quad Pmmm(\bar{3})11 \tag{3}$$

The OD packet can be taken to consist of half the OD layer M' and the OD layer L' (Fig. 10), so that the structure can be described with the alternate stacking of the OD packet P_{2n} and P_{2n+1}, which are related with each other by inversion symmetry (with respect to the origin of the OD layer M'). The boundary between two adjacent OD packets is set so that R and T atoms in the OD layer L' highlighted with green and orange color in Fig. 11(a) and those in the OD layer M' highlighted with dark green and brown colors in Fig. 11(a) belong to both OD packets. The OD packet projected along the stacking direction and symbolic figure for the OD packet are shown in Figs. 11(b) and (c), respectively.

The origin of the adjacent packet P_{2n+1} may be shifted relative to that of the packet P_{2n} by either of the following stacking vectors,

$$\boldsymbol{t}_1 = \boldsymbol{c}_0 \tag{4a}$$

$$\boldsymbol{t}_2 = \frac{2}{3}\boldsymbol{a}_1 + \frac{1}{3}\boldsymbol{a}_2 + \boldsymbol{c}_0 \qquad (4b)$$

where $\boldsymbol{c}_0$ corresponds to the unit vector of the OD packet along the stacking direction. In the former case, the packet P_{2n+1} is stacked right above the packet P_{2n} after ±60 or 180° rotation about the *c*-axis ($A_{\uparrow} \rightarrow A'_{\downarrow}$: Fig. 11(d))[2]. In the latter case, the packet P_{2n+1} is stacked obliquely

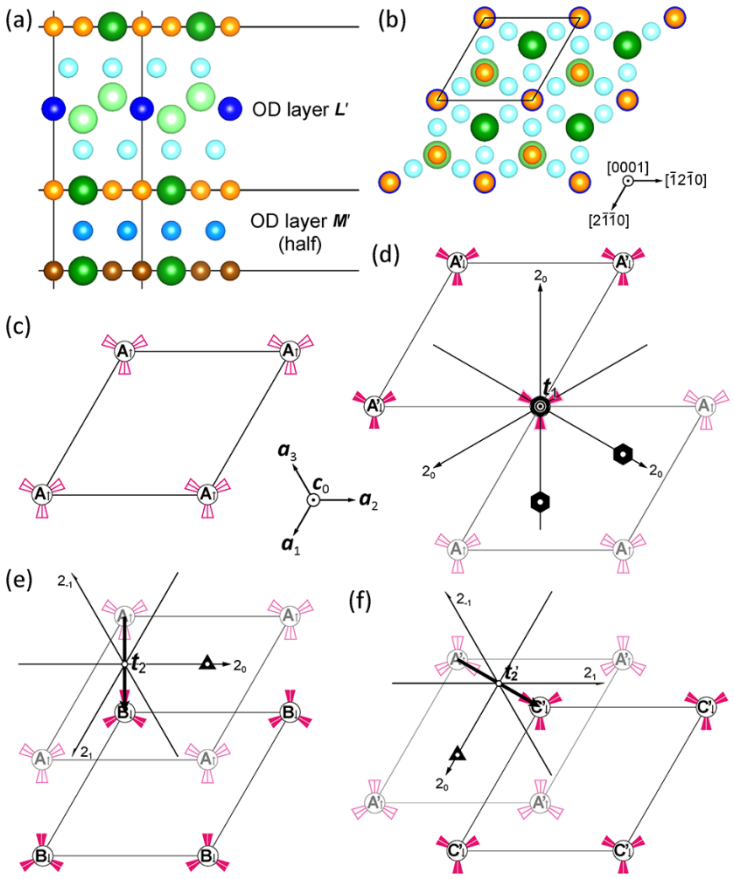

Figure 11. (a) [$2\bar{1}\bar{1}0$] and (b) [0001] projections of the OD packet in the $(Nd,Mg)_2(Ni,Al)_7$ phase of the new crystal structure. (c) Arrays of symbolic figures showing the symmetry of the OD packet. (d,e) Two different manners of stacking the adjacent OD packet on the preceding OD packet at the position $A_{\uparrow}$. (d) $A_{\uparrow} \rightarrow A'_{\downarrow}$ with the

[2]The upward and downward arrows indicate that the OD layer *L'* is located on the top or in the bottom of the OD packet, respectively (see Figure 10).

stacking vector $\boldsymbol{t}_1$, (e) $A_{\uparrow} \rightarrow B_{\downarrow}$ with the stacking vector $\boldsymbol{t}_2$. (f) One of the two manners of stacking the adjacent OD packet on the preceding OD packet at the position $A'_{\uparrow}$ ($A'_{\uparrow} \rightarrow C'_{\downarrow}$).

above the packet P_{2n} without rotation ($A_{\uparrow} \rightarrow B_{\downarrow}$: Fig. 11(e)). When the packet P_{2n} has a different orientation (±60 or 180° rotation about the *c*-axis; $A'_{\uparrow}$ position), the packet P_{2n+1} can be stacked right above the packet P_{2n} after ±60 or 180° rotation about the *c*-axis ($A'_{\uparrow} \rightarrow A_{\downarrow}$), after shifting the origin by the following stacking vector,

$$\boldsymbol{t}'_1 = \boldsymbol{c}_0 , \tag{4c}$$

or obliquely above the packet P_n without rotation ($A'_{\uparrow} \rightarrow C'_{\downarrow}$: Fig. 11(f)) after shifting the origin by the following stacking vector,

$$\boldsymbol{t}'_2 = \frac{1}{3}\boldsymbol{a}_1 + \frac{2}{3}\boldsymbol{a}_2 + \boldsymbol{c} . \tag{4d}$$

The stacking vector $\boldsymbol{t}_1$ shifts the positions like $A_{\uparrow} \rightarrow A'_{\downarrow}$, $B_{\uparrow} \rightarrow B'_{\downarrow}$, $C_{\uparrow} \rightarrow C'_{\downarrow}$, while $\boldsymbol{t}_2$ and $\boldsymbol{t}'_2$ shift the positions like $A_{\uparrow} \rightarrow B_{\downarrow}$, $B_{\uparrow} \rightarrow C_{\downarrow}$, $C_{\uparrow} \rightarrow A_{\downarrow}$, and $A'_{\uparrow} \rightarrow C'_{\downarrow}$, $B'_{\uparrow} \rightarrow A'_{\downarrow}$, $C'_{\uparrow} \rightarrow B'_{\downarrow}$, respectively. An infinite number of periodic and non-periodic polytypes can be obtained by a random occurrence of the stacking vectors $\boldsymbol{t}_i$ and $\boldsymbol{t}'_i$ (i = 1 and 2) similarly for R_2T_7 formed based on the stacking of the structural block consisting of a sub-block layer of the RT_3 stoichiometry (formed with one R_2T_4 unit layer and one RT_5 unit layer) and a sub-block layer of the R_5T_{19} stoichiometry (formed with one R_2T_4 unit layer and three RT_5 unit layers).

A similar argument holds true in deducing the MDO polytypes. In the case of the OD groupoid family for the R_2T_7 phase with the new crystal structure, one generating operation is the σ-PO of 6_6, indicated in Fig. 11(d). Continuous application of this operation yields an MDO

polytype (MDO1) with the $A_{\uparrow}A'_{\downarrow}$ stacking sequence. The unit cell of the MDO1 polytype

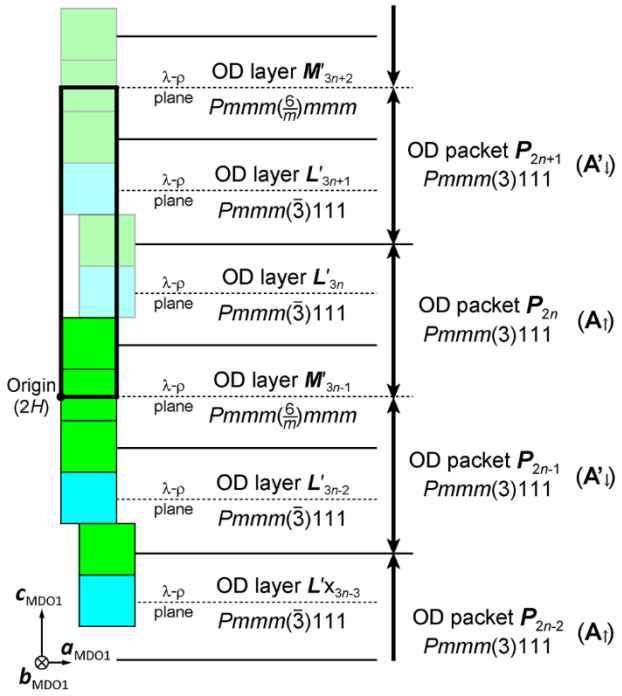

Figure 12. Schematic illustration of the (imaginary) crystal structure of the intermetallic compound $(Nd,Mg)_2(Ni,Al)_7$ (2*H*-polytype). The constituting OD layers and packets are described in the right-hand of the figure.

belongs to the space group of $P\bar{6}m2$ with a hexagonal unit cell of $\boldsymbol{a}_1^{(MDO1)} = \boldsymbol{a}_1$, $\boldsymbol{a}_2^{(MDO1)} = \boldsymbol{a}_2$ and $\boldsymbol{c}^{(MDO1)} = 2\boldsymbol{c}_0$ because the σ-PO of 6_6 becomes a total operation, $\bar{6}^+$, in the hexagonal cell (Fig. 12). In the Ramsdell notation, the MDO1 polytype is designated 2*H*. Another generating operation is the σ-PO of $\bar{3}$ indicated in Fig. 11(e). Continuous application of this operation results in another MDO polytype (MDO2) with the $A_{\uparrow}B_{\downarrow}C_{\uparrow}A_{\downarrow}B_{\uparrow}C_{\downarrow}$ stacking sequence (Fig. 8). The MDO2 polytype belongs to the space group of $R\bar{3}m$ with the rhombohedral unit cell of $\boldsymbol{a}_1^{(MDO2)} = \boldsymbol{a}_1$, $\boldsymbol{a}_2^{(MDO2)} = \boldsymbol{a}_2$, and $\boldsymbol{c}^{(MDO2)} = 6\boldsymbol{c}_0$ because the σ-PO of $\bar{3}$ becomes a total operation $g(1/6, 1/3, 1/3)$ in the rhombohedral cell. In the Ramsdell notation, the MDO2 polytype is designated 6*R*. The experimentally observed polytype is $R\bar{3}m$ (MDO2), which is the second

simplest polytype in the OD family. Of importance to note here is that the actual number of block layers in the unit cell for the 6*R* polytype is six ($A_{\uparrow}B_{\downarrow}C_{\uparrow}A_{\downarrow}B_{\uparrow}C_{\downarrow}$) but not three (ABC), if we take into account of the inversion symmetry between two neighboring block layers on their stacking.

4.3. Stacking faults and electron diffraction

Diffraction from OD structures usually produces two different types of reflections; family reflections and characteristic reflections [20, 34]. Family reflections appear at the common positions for all polytypes if they belong to the same OD family, while characteristic reflections appear at different positions specific to a given polytype, with which polytype identification is possible. If some different polytypes are incorporated or if some stacking disorder is present, sharp streaks are observed in the reciprocal lattice rows of characteristic reflections while discrete diffraction spots are preserved for family reflections, as far as the stacking made is only those allowed to form the same OD family [21, 35]. On the other hand, if some different phases are incorporated in the form of intergrowth or if some stacking disorder that is not allowed to form the same OD family occurs, streaks are observed in the reciprocal lattice rows of both family and characteristic reflections.

The reflection conditions for the family reflections can be obtained by considering reflection conditions for the so-called 'family structure', a fictitious superimposed structure that is obtained by simultaneous application of all possible σ-POs [20, 21, 35]. The reflection conditions for the family reflections of R_2T_7 with the new crystal structure are described as follows:

$$0H\overline{H}L : H = 3m,\ L = 3n\ (m,n : \text{integer}) \qquad (5)$$

where the indices in capital letters refer to the unit cell of the MDO2 (6*R*) polytype. Indexing of the SAED patterns of Fig. 3(b) was made assuming the MDO2 (6*R*) polytype. Calculation of SAED patterns with the $[2\bar{1}\bar{1}0]$ incidence indicates that the $m[01\bar{1}L]$* reciprocal lattice rows ($m = 3n$, where m and n are integers) correspond to those of family reflections, while the $m[01\bar{1}L]$* reciprocal lattice rows ($m \neq 3n$) to those of characteristic reflections. Although the intensity is fairly low, streaks are observed in Fig. 3(b) along reciprocal lattice rows of both family and characteristic reflections. This indicates either the incorporation of some different phases in the form of intergrowth or the introduction of some stacking disorder that is not allowed to form the same OD family. When judged from the HAADF-STEM image of Fig. 4, the intergrowth structures, in which, for example, a sub-block layer of either RT_3 or R_5T_{19} stoichiometry is missed (SF's 1 and 2 in Fig. 4), are identified to be responsible for the occurrence of streaks. In other words, R_2T_7 with the new crystal structure is relatively stable with respect to other polytype, since the incorporation of other polytypes is less frequent.

4.4. Further possible crystal structures with different stoichiometric compositions and with different stacking structures

A series of compounds in the *R*-*T* system, RT_3, R_2T_7 and R_5T_{19} possess a crystal structure based on the stacking of block layers, each of which has their own stoichiometric composition consisting of one unit layer of the R_2T_4 (Laves)-type and some unit layers of the RT_5-type [12-14, 36] (Fig. 1). As the number (n) of RT_5-type unit layers in the block layer increases, intermetallics richer in *T* (n=1, 2 and 3 for RT_3, R_2T_7 and R_5T_{19}, respectively) are successively formed so as to be formulated as RT_x with $x=(5n+4)/(n+2)$ [12]. Theoretically, it is possible to form intermetallic compounds RT_x with the value of n exceeding 4 (RT_4, R_7T_{29} and

R_4T_{17} for, n=4, 5 and 6, respectively). Although these intermetallics with higher x values have never been reported in the R-T binary system, the intermetallic compound RT_4 (La_5MgNi_{24}) with n=4 has indeed been reported to form in the La-Mg-Ni ternary system [37]. The intermetallic compound RT_4 is reported to exhibit better discharge capacity than that based on R_5T_{19} when examined as a negative electrode of Ni-MH batteries [37].

The new crystal structure of R_2T_7 presently identified is different from those of these intermetallics RT_x with higher x values in that although the structure is formed similarly based on the stacking of block layers, the block layer for the new crystal structure consists of one sub-block layer of the RT_3 stoichiometry (formed with one R_2T_4 unit layer and one RT_5 unit layer) and one sub-block layer of the R_5T_{19} stoichiometry (formed with one R_2T_4 unit layer and three RT_5 unit layers), which alternately stack on top of each other. If the block layer is allowed to consist of more than two kinds of sub-block layers (either of RT_3, R_2T_7 or R_5T_{19} stoichiometry), it is possible to form an infinite number of intermetallic compounds at stoichiometric compositions in between RT_2 and RT_5. Although the stoichiometric composition of the new structure formed with one sub-block layer of the RT_3 stoichiometry and one sub-block layer of the R_5T_{19} stoichiometry is R_2T_7, the stoichiometric composition is changed to R_7T_{23} if the sub-block layer of the R_5T_{19} stoichiometry is replaced with that of the R_2T_7 stoichiometry (Fig. 13(b)). This crystal structure of R_7T_{23} ($La_5Mg_2Ni_{23}$) has indeed been observed to exist in the La-Mg-Ni ternary system [1, 38]. The intermetallic compound R_7T_{23} is reported also to exhibit better discharge capacity than that based on RT_5 [1]. Similarly, the intermetallic compound R_3T_{11} is formed with the block layer consisting of one R_2T_7 sub-block layer and one R_5T_{19} sub-block layer (Fig. 13(c)). Another crystal structure of the intermetallic compound R_2T_7 is formed with the block layer consisting of one RT_3 sub-block layer, one R_2T_7 sub-block layer and one

R_5T_{19} sub-block layer (Fig. 13(d)). If the block layer consists of two RT_3 sub-block layers and either R_2T_7 or

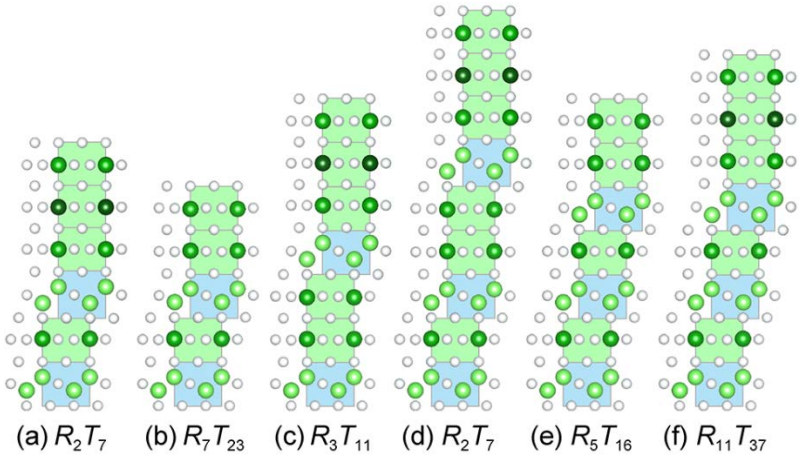

Figure 13. Further possible crystal structures with different stoichiometric compositions and with different stacking structures.

R_5T_{19} sub-block layer, the stoichiometric composition is either R_5T_{16} (Fig. 13(e)) or $R_{11}T_{37}$ (Fig. 13(f)). Needless to say, all these crystal structures can be described with the OD theory (as described in Sections 4.1 and 4.2), as far as they are based on the stacking of block layers.

The crystal structure variation as mentioned above is empirically known not to occur in simple *R*-*T* systems, unless Mg is added to replace some *R* atoms [1, 37-41]. In this sense, Mg is considered to play an important role in controlling the stability of crystal structures. Electrochemical properties of intermetallic compounds RT_x containing Mg have frequently been reported to be better than those of their base compounds [3, 7, 8, 11, 42-46]. Our preliminary experiment has indicated that the alloy 2 containing grains of the R_2T_7 phase with the new crystal structure tends to exhibit better discharge capacity than the alloy 1 containing grains of the R_2T_7 phase with the conventional 2*H* polytype structure (See the Supplementary Figure S1). Their properties cannot simply be inferred from the rule of mixture of the intermetallic compounds R_2T_4 and RT_5 that constitute the block layer [11, 42, 45]. This indicates that there is

a chance to find out a new compound that exhibits excellent electrochemical properties as a negative electrode of Ni-MH batteries through controlling crystal structures based on the stacking of block layers with additions of Mg and some other alloying elements. Mg is reported to preferentially occupy *R* atom sites in the R_2T_4 unit layer of the block layer in a series of compounds RT_x in the *R*-*T* system. In the presence of a quaternary element that has preferential occupancy in particular sites in either R_2T_4 or RT_5 unit layer, there is a possibility that the occupancy behavior of Mg in the R_2T_4 unit layer varies with sub-block layers if the block layer consists of sub-block layers with different stoichiometric compositions, as in the presently identified new crystal structure of R_2T_7. We believe that Al is one of the effective quaternary elements that also play an important role, since Al has been known to preferentially occupy *T* sites between R_2T_4 and RT_5 unit layers and between RT_5 unit layers [37]. Indeed, the present study clearly indicates that crystal grains of the R_2T_7 phase with the new crystal structure tend to possess more Mg and Al than those of the R_2T_7 phase with the conventional 2*H* polytype structure. Ways to control the constitution and stacking of block layers of the intermetallic compounds RT_x correlating with the occupancy behavior of Mg and other alloying elements are currently under survey experimentally and theoretically in our research group.

5. CONCLUSIONS

(1) The new crystal structure of the intermetallic compound $(Nd,Mg)_2(Ni,Al)_7$ has been determined as that based on the stacking of the block layer of the R_2T_7 stoichiometry that consists of a sub-block layer of the RT_3 stoichiometry (formed with one R_2T_4 unit layer and one RT_5 unit layer) and a sub-block layer of the R_5T_{19} stoichiometry (formed with one R_2T_4 unit layer and three RT_5 unit layers), which alternately stack on top of each other in the stacking of

the ABC-type. This is quite different from the crystal structures (either 2*H* or 3*R* polytypes) usually reported for the intermetallic compound R_2T_7, in which the block layer of the R_2T_7 stoichiometry consists simply of one R_2T_4 unit layer and two RT_5 unit layers.

(2) The new crystal structure is described based on the order-disorder theory. The crystal structure belongs to the category IV OD structure composed of two types of non-polar OD layers (L' and M'). Due to the selectivity property of the orientation of the OD layer L', there are two possible equivalent positions to stack an OD layer L' on top of an OD layer L' or M'. The OD groupoid family symbol expressing the OD structure is:

$$Pmmm\left(\frac{6}{m}\right)mmm \quad Pmmm(\bar{3})11 \quad Pmmm(\bar{3})11$$

$$[2/3, 1/3] \qquad [2/3, 1/3]$$

(3) The space groups for the two simplest forms (MDO polytypes) of the intermetallic compound R_2T_7 are determined to be $P\bar{6}m2$ (MDO1) and $R\bar{3}m$ (MDO2). In the Ramsdell notation, these forms are designated 2*H* and 6*R*, respectively. The experimentally observed polytype is $R\bar{3}m$ (MDO2), which is the second simplest polytype in the OD family.

ACKNOWLEDGMENT

This work was supported by JSPS KAKENHI grant numbers 24246113 and 25709066, and the Elements Strategy Initiative for Structural Materials (ESISM) from the Ministry of Education, Culture, Sports, Science and Technology (MEXT) of Japan, and in part by Advanced Low Carbon Technology Research and Development Program (ALCA) from the Japan Science and Technology Agency (JST).

REFERENCES

[1] Kohno T, Yoshida H, Kawashima F, Inaba T, Sakai I, Yamamoto M, et al. Hydrogen storage properties of new ternary system alloys: La_2MgNi_9, $La_5Mg_2Ni_{23}$, La_3MgNi_{14}. J Alloys Compd. 2000;311:L5-L7.
[2] Akiba E, Hayakawa H, Kohno T. Crystal structures of novel La-Mg-Ni hydrogen absorbing alloys. J Alloys Compd. 2006;408:280-3.
[3] Zhang FL, Luo YC, Wang DH, Yan RX, Kang L, Chen JH. Structure and electrochemical properties of $La_{2-x}Mg_xNi_{7.0}$ (x=0.3-0.6) hydrogen storage alloys. J Alloys Compd. 2007;439:181-8.
[4] Denys RV, Riabov AB, Yartys VA, Sato M, Delaplane RG. Mg substitution effect on the hydrogenation behaviour, thermodynamic and structural properties of the La_2Ni_7-$H(D)_2$ system. J Solid State Chem. 2008;181:812-21.
[5] Yartys VA, Vajeeston P, Riabov AB, Ravindran P, Denys RV, Maehlen JP, et al. Crystal chemistry and metal-hydrogen bonding in anisotropic and interstitial hydrides of intermetallics of rare earth (R) and transition metals (T), $RT3$ and R_2T_7. Z Kristallogr. 2008;223:674-89.
[6] Crivello JC, Zhang J, Latroche M. Structural Stability of AB_y Phases in the (La,Mg)-Ni System Obtained by Density Functional Theory Calculations. J Phys Chem C. 2011;115:25470-8.
[7] Liu YF, Cao YH, Huang L, Gao MX, Pan HG. Rare earth-Mg-Ni-based hydrogen storage alloys as negative electrode materials for Ni/MH batteries. J Alloys Compd. 2011;509:675-86.
[8] Zhang QG, Zhao B, Fang MH, Liu CR, Hu QM, Fang F, et al. $(Nd_{1.5}Mg_{0.5})Ni_7$-Based Compounds: Structural and Hydrogen Storage Properties. Inorg Chem. 2012;51:2976-83.
[9] Serin V, Zhang JX, Magen C, Serra R, Hytch MJ, Lemort L, et al. Identification of the atomic scale structure of the $La_{0.65}Nd_{0.15}Mg_{0.20}Ni_{3.5}$ synthesized by spark plasma sintering alloy. Intermetallics. 2013;32:103-8.
[10] Yasuoka S, Magari Y, Murata T, Tanaka T, Ishida J, Nakamura H, et al. Development of high-capacity nickel-metal hydride batteries using superlattice hydrogen-absorbing alloys. J Power Sources. 2006;156:662-6.
[11] Oesterreicher H, Clinton J, Bittner H. Hydrides of La-Ni Compounds. Mater Res Bull. 1976;11:1241-7.
[12] Khan Y. Constitution of R-T Systems (R=Rare Earths and Yttrium, T=Iron, Cobalt and Nickel). Z Metallkd. 1974;65:489-95.
[13] Takeda S, Kitano Y, Komura Y. Polytypes of the Intermetallic Compound Sm_5Ni_{19}. J Less-Common Met. 1982;84:317-25.
[14] Takeda S, Horikoshi H, Komura Y. Microstructure of Sm_5Ni_{19} Intermetallic Compound Observed by High-Resolution Electron-Microscope. Journal of Microscopy-Oxford. 1983;129:347-58.
[15] Ramsdell LS. Studies on Silicon Carbide. Am Mineral. 1947;32:64-82.
[16] Dornberger-Schiff K. On Order-Disorder Structures (OD-Structures). Acta Crystallogr. 1956;9:593-601.
[17] Dornberger-Schiff K. On the Nomenclature of the 80 Plane Groups in 3 Dimensions. Acta Crystallogr. 1959;12:173-.
[18] Dornberger-Schiff, K. Grundzüge einer Theorie der OD-Strukturen aus Schichten. Abh Dtsch Akad Wiss. 1964;3:1-107.
[19] Dornberger-Schiff K. OD Structures, — a Game and a Bit More. Krist Techn. 1979;14:1027-45.
[20] Ďurovič S. Fundamentals of the OD theory. In: Merlino S, editor. Modular Aspects of

Minerals. Budapest, Hungary: Eőtvős University Press; 1997. p. 3-28.
[21] Ferraris G, Makovicky E, Merlino S. Crystallography of Modular Materials. Oxford, UK: Oxford University Press; 2008.
[22] Jeffery JW. Unusual X-Ray Diffraction Effects from a Crystal of Wollastonite. Acta Crystallogr. 1953;6:821-5.
[23] Dornbergerschiff K, Liebau F, Thilo E. Zur Struktur Des Beta-Wollastonits, Des Maddrellschen Salzes Und Des Natriumpolyarsenats. Acta Crystallogr. 1955;8:752-4.
[24] Yokobayashi H, Kishida K, Inui H, Yamasaki M, Kawamura Y. Enrichment of Gd and Al atoms in the quadruple close packed planes and their in-plane long-range ordering in the long period stacking-ordered phase in the Mg-Al-Gd system. Acta Mater. 2011;59:7287-99.
[25] Kishida K, Yokobayashi H, Inui H, Yamasaki M, Kawamura Y. The crystal structure of the LPSO phase of the 14H-type in the Mg-Al-Gd alloy system. Intermetallics. 2012;31:55-64.
[26] Kishida K, Yokobayashi H, Inui H. The most stable crystal structure and the formation processes of an order-disorder (OD) intermetallic phase in the Mg-Al-Gd ternary system. Philos Mag. 2013;93:2826-46.
[27] Okamoto NL, Yasuhara A, Inui H. Order-Disorder Structure of the δ_{1k} Phase in the Fe–Zn System Determined by Scanning Transmission Electron Microscopy. Acta Mater. 2014;81:345-57.
[28] Kopsky V, Litvin DB. International Tables for Crystallography, Vol. E: Superperiodic group. 2nd ed. Chichester, UK: John Wiley & Sons, Ltd; 2010.
[29] Dornbergerschiff K, Grell H. Geometrical Properties of MDO Polytypes and Procedures for Their Derivation: OD Families Containing OD Layers of M Greater-Than 1 Kinds and Their MDO Polytypes. Acta Crystallogr A. 1982;38:491-8.
[30] Grell H, Dornbergerschiff K. Symbols for OD Groupoid Families Referring to OD Structures (Polytypes) Consisting of More Than One Kind of Layer. Acta Crystallogr A. 1982;38:49-54.
[31] Merlino S, Orlandi P, Perchiazzi N, Basso R, Palenzona A. Polytypism in Stibivanite. Can Mineral. 1989;27:625-32.
[32] Durovic S. Notion of Packets in Theory of OD Structures of M Greater-Than 1 Kinds of Layers - Examples - Kaolinites and MoS_2. Acta Crystallogr B. 1974;30:76-8.
[33] Hybler J, Durovic S. The OD interpretation of the crystal structure of kettnerite $CaBiOFCO_3$. Acta Crystallogr A. 2009;65:501-11.
[34] Durovic S, Hybler J. OD structures in crystallography - basic concepts and suggestions for practice. Z Kristallogr. 2006;221:63-76.
[35] Merlino S. OD approach in ninerals: examples and applications. In: Merlino S, editor. Modular Aspects of Minerals. Budapest, Hungary: Eőtvős University Press; 1997. p. 29-54.
[36] Iwase K, Mori K. Crystal structure and hydrogen storage property of Nd_2Ni_7 superlattice alloy. Int J Hydrogen Energy. 2013;38:5316-21.
[37] Ozaki T, Kanemoto M, Kakeya T, Kitano Y, Kuzuhara M, Watada M, et al. Stacking structures and electrode performances of rare earth-Mg-Ni-based alloys for advanced nickel-metal hydride battery. J Alloys Compd. 2007;446:620-4.
[38] Kohno T, Takeno S, Yoshida H, Kanda M. Structural analysis of La-Mg-Ni-based new hydrogen storage alloy. Res Chem Intermed. 2006;32:437-45.
[39] Yamamoto T, Inui H, Yamaguchi M, Sato K, Fujitani S, Yonezu I, et al. Microstructures and hydrogen absorption/desorption properties of La-Ni alloys in the composition range of La-77.8~83.2 at.%Ni. Acta Mater. 1997;45:5213-21.

[40] Inui H, Yamamoto T, Di Z, Yamaguchi M. Microstructures and defect structures in intermetallic compounds in the La-Ni alloy system. J Alloys Compd. 1999;293:140-5.
[41] Di Z, Yamamoto T, Inui H, Yamaguchi M. Characterization of stacking faults on basal planes in intermetallic compounds La_5Ni_{19} and La_2Ni_7. Intermetallics. 2000;8:391-7.
[42] Oesterreicher H, Bittner H. Hydride Formation in $La_{1-x}Mg_xNi_2$. J Less-Common Met. 1980;73:339-44.
[43] Kadir K, Kuriyama N, Sakai T, Uehara I, Eriksson L. Structural investigation and hydrogen capacity of $CaMg_2Ni_9$: a new phase in the AB_2C_9 system isostructural with $LaMg_2Ni_9$. J Alloys Compd. 1999;284:145-54.
[44] Tang R, Liu YN, Zhu CC, Zhu JW, Yu G. Effect of Mg on the hydrogen storage characteristics of $MI_{1-x}Mg_xNi_{2.4}Co_{0.6}$ (x=0-0.6) alloys. Mater Chem Phys. 2006;95:130-4.
[45] Terashita N, Akiba E. Hydriding properties of $(Mg_{1-x}M_x)Ni_2$ C15-type laves phase alloys. Mater Trans. 2006;47:1890-3.
[46] Dong XP, Lu FX, Yang LY, Zhang YH, Wang XL. Influence of spark plasma sintering temperature on electrochemical performance of $La_{0.80}Mg_{0.20}Ni_{3.75}$ alloy. Mater Chem Phys. 2008;112:596-602.

Figure 1. Crystal structures of (a) RT_2 (R_2T_4), (b) RT_3, (c) R_2T_7, (d) R_5T_{19} and (e) RT_5. RT_2 and RT_5 have C15 (Laves)- and $CaCu_5$-type structures, respectively. The crystal structures of (b) RT_3, (c) R_2T_7 and (d) R_5T_{19} consist of block layers, each of which consists of R_2T_4 and RT_5 unit layers, and the polytype *2H* is illustrated for these intermetallics.

Figure 2. (a) Typical high-resolution HAADF-STEM image and (b) SAED pattern with the $[2\bar{1}\bar{1}0]$ incidence for a crystal grain of the R_2T_7 phase in the alloy 1. Positions of sub-block layers of the RT_5- and R_2T_4-types are indicated in the figure.

Figure 3. (a) Typical high-resolution HAADF-STEM image and (b) SAED pattern with the $[2\bar{1}\bar{1}0]$ incidence for a crystal grain of the R_2T_7 phase in the alloy 2. Positions of sub-block layers of the RT_3- and R_5T_{19}-types are indicated in the figure.

Figure 4. Low-magnification HAADF-STEM image of the R_2T_7 phase in the alloy 1. Positions of stacking faults (SF1 and SF2) are indicated in the right of the figure.

Figure 5. Crystal structures of (a) 2*H*-RT_3, (b) 2*H*-R_2T_7, and (c) 2*H*-R_5T_{19} projected along the $[2\bar{1}\bar{1}0]$ direction. The constituting OD layers and packets are described in the right-hand of each figure.

Figure 6. (a,c,d,e) $[2\bar{1}\bar{1}0]$ and (b,f) [0001] projections of the OD layers (a,b) *L* and (c,d,e) *M*, respectively, in the (c) RT_3, (d) R_2T_7, and (e) R_5T_{19} phases. (g,h) Diagrams of symmetry elements for the $p\bar{3}m1$ and $p6/mmm$ layer groups corresponding to the λ-POs in the OD layers *L* and *M*, respectively.

Figure 7. (a) $[2\bar{1}\bar{1}0]$ and (b) [0001] projections of the OD packet in the R_2T_7 phase. (c) Arrays of symbolic figures showing the symmetry of the OD packet. (d,e) Two different manners of stacking the adjacent OD packet on the preceding OD packet at the position A. (d) A⇒A' with the stacking vector $\boldsymbol{t}_1$, (e) A⇒B with the stacking vector $\boldsymbol{t}_2$. (f) One of the two manners of stacking the adjacent OD packet on the preceding OD packet at the position A' (A'⇒C').

Figure 8. Schematic illustration of the crystal structure of the intermetallic compound $(Nd,Mg)_2(Ni,Al)_7$ (6*R*-polytype). The constituting OD layers and packets are described in the right-hand of the figure.

Figure 9. (a,c) $[2\bar{1}\bar{1}0]$ and (b,d) [0001] projections of the OD layers (a,b) *L'* and (c,d) *M'*, respectively, in the $(Nd,Mg)_2(Ni,Al)_7$ phase of the new crystal structure.

Figure 10. Schematic illustration of the OD packets P_{2n} and P_{2n+1} constituting the $(Nd,Mg)_2(Ni,Al)_7$ phase of the new crystal structure.

Figure 11. (a) $[2\bar{1}\bar{1}0]$ and (b) [0001] projections of the OD packet in the $(Nd,Mg)_2(Ni,Al)_7$ phase of the new crystal structure. (c) Arrays of symbolic figures showing the symmetry of the OD packet. (d,e) Two different manners of stacking the adjacent OD packet on the preceding OD packet at the position $A_\uparrow$. (d) $A_\uparrow \rightarrow A'_\downarrow$ with the stacking vector $\boldsymbol{t}_1$, (e) $A_\uparrow \rightarrow B_\downarrow$ with the stacking vector $\boldsymbol{t}_2$. (f) One of the two manners of stacking the adjacent OD packet on the preceding OD packet at the position $A'_\uparrow$ ($A'_\uparrow \rightarrow C'_\downarrow$).

Figure 12. Schematic illustration of the (imaginary) crystal structure of the intermetallic compound $(Nd,Mg)_2(Ni,Al)_7$ (2*H*-polytype). The constituting OD layers and packets are described in the right-hand of the figure.

Figure 13. Further possible crystal structures with different stoichiometric compositions and with different stacking structures.

Table 1. Nominal compositions of the alloys 1 and 2.

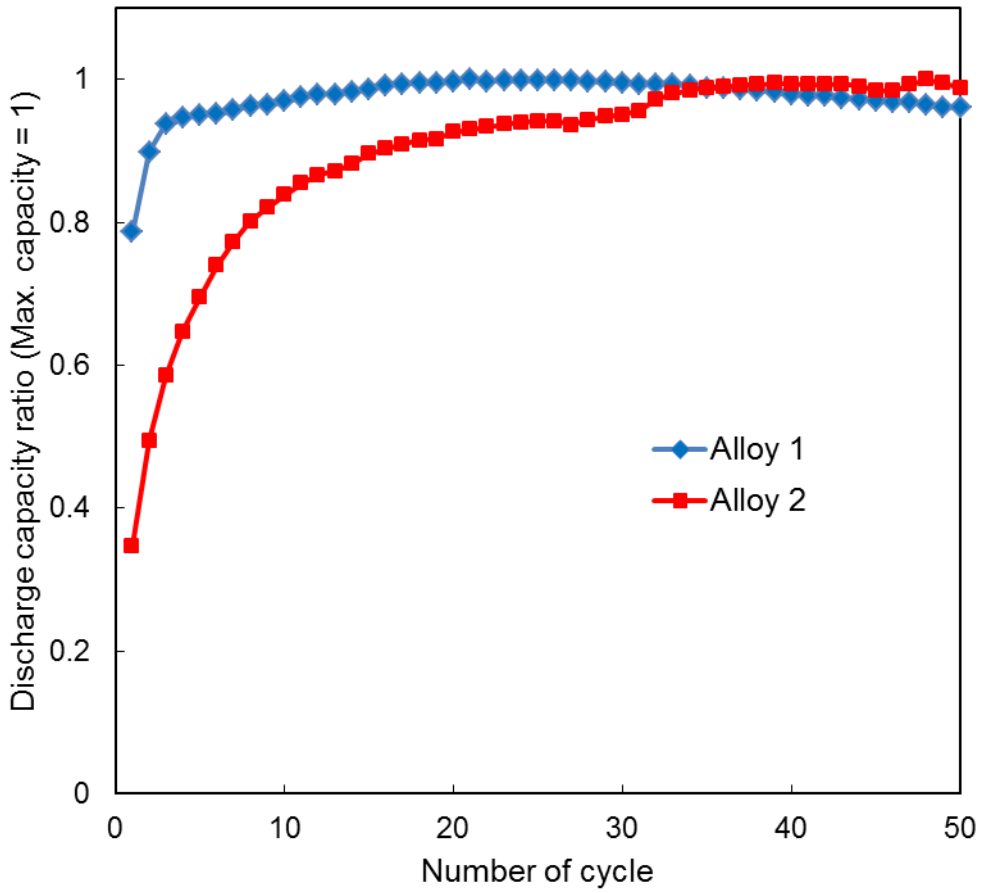

Figure S1: Charge/discharge cycle dependence of discharge capacities ratio (max. capacity = 1) of three-electrode test cells using negative electrodes of the alloy 1 and 2.

.

Figure indicates variations in the discharge capacity ratio (maximum capacity = 1) with respect to the number of charge/discharge cycles. After 50 charge/discharge cycles, the cell using a negative electrode of the alloy2 exhibit a higher discharge capacity ratio than that with the alloy 1 electrode, which indicates better cycle behavior of the negative electrode of the alloy 2.

For the evaluation of the discharge capacity, a three-electrode test cell composed of a Nd-Mg-Ni-Al alloy electrode, a counter electrode of sintered nickel electrode, an Hg/HgO reference electrode, and electrolyte of a 30 mass% KOH aqueous solution. Pellet-type negative electrodes of the Nd-Mg-Ni-Al alloy was prepared from a mixture of the quaternary alloy and Ni powders and compressed under pressure of 150 MPa. The test cell was charged at 150 mA g^{-1} for 2 h and 50 min and discharged at 150 mA g^{-1} until the negative electrode potential reached −0.7 V with respect to the reference electrode.